J Eng Math (2008) 62:35–50
DOI 10.1007/s10665-007-9185-z

Linear shear flow past a hemispherical droplet adhering to a solid surface

K. Sugiyama · M. Sbragaglia

Received: 4 December 2006 / Accepted: 6 August 2007 / Published online: 1 September 2007

Abstract The properties of a three-dimensional shear flow overpassing a hemispherical droplet resting on a plane wall are investigated. The exact solution is computed as a function of the viscosity ratio between the droplet and the surrounding fluid and generalizes the solution for the hemispherical no-slip bump given in an earlier paper by Price (*QJMAM* (1985) 38: 93–104). Several expressions, including the torque and the force acting on the drop, are considered as well as the importance of the deformations on the surface for small capillary numbers.

Keywords Droplets · Droplet deformations · Laminar shear flows

1 Introduction

A detailed description of shear flows past viscous droplets resting on a plane wall is necessary for understanding and modelling a series of engineering, physiological and natural situations [1]. Examples include bubble growth and detachment from heated walls [2,3], drop removal and dislocation in detergency problems [4] and also membrane emulsification, where a liquid is pumped into another, shearing droplets and consequently forming emulsions. Pertinent physiological applications can also be included, such as the growth of thrombosis and also a tentative description of the deformation and dislodging of white and red blood cells adhering to the endothelium.

Shear flows over protuberances have already been considered previously; O'Neill [5] derived an infinite-series solution for the flow over a full sphere in contact with a wall, while Hyman [6] and Price [7] derived a solution for the case of hemispherical no-slip bumps, a problem regarded as a limiting case for highly viscous droplets. Pozrikidis [8] provided an accurate description of shear flows over protuberances projecting from a plane surface using the boundary-integral method. A considerable number of papers have also described drop-displacement problems [9–13] and their variations: Yon et al. [14,15] studied shear-induced deformations of droplets with fixed contact lines and the work of Schleizer [16] tackled the problem in both pressure-driven and shear flows. More recently, also inertial effects past pinned droplets have been considered [17].

In this paper we derive an exact solution for the case of an incompressible shear flow overpassing a hemispherical droplet of arbitrary viscosity. This solution will be computed as a function of the viscosity ratio between the droplet

K. Sugiyama · M. Sbragaglia (✉)
Faculty of Applied Sciences, IMPACT, and Burgerscentrum, University of Twente, P.O. Box 217, AE 7500 Enschede, The Netherlands
e-mail: sbragaglia@roma2.infn.it

and the fluid and is the natural generalization of the one proposed by Price [7], here recovered in the limit of a highly viscous droplet. Several analytical expressions, including the force and torque acting on the droplet, will be given. Moreover, in the limit of small capillary numbers, the role of surface deformations will be investigated and a comparison with available numerical data will be presented.

2 Formulation of the problem

We consider the motion of a viscous incompressible fluid with velocity $\mathbf{v}$, of constant density ρ and dynamical viscosity η, close to a solid plane boundary. Under the assumption of small Reynolds numbers, this motion is reasonably approximated by a uniform shear flow whose magnitude will be denoted by S. We will consider how this flow is disturbed by a hemispherical drop of radius R and density $\hat{\rho}$ on the plane boundary. We will use polar coordinates (r, θ, ϕ) with the origin in the center of the hemisphere and an x-axis in the direction of the shear flow (see Fig. 1 for details). The flow inside the drop will be identified with a velocity $\hat{\mathbf{v}}$ and viscosity $\hat{\eta}$ in a prescribed ratio with respect to the outer viscosity. This ratio will be denoted by $\lambda = \hat{\eta}/\eta$. Indicating by p and $\hat{p}$ the outer and inner pressure, respectively, we may write the continuity and Stokes equations as follows:

$$\nabla \cdot \mathbf{v} = \nabla \cdot \hat{\mathbf{v}} = 0, \tag{1}$$

$$\nabla \cdot \boldsymbol{\sigma} = \nabla \cdot \hat{\boldsymbol{\sigma}} = 0, \tag{2}$$

where

$$\boldsymbol{\sigma} = -p\mathbf{I} + \eta\left(\nabla\mathbf{v} + (\nabla\mathbf{v})^T\right), \quad \hat{\boldsymbol{\sigma}} = -\hat{p}\mathbf{I} + \hat{\eta}\left(\nabla\hat{\mathbf{v}} + (\nabla\hat{\mathbf{v}})^T\right). \tag{3}$$

We will assume no-slip boundary conditions on the wall:

$$\mathbf{v} = 0 \quad r \geq R,\ \theta = \frac{\pi}{2}, \quad 0 \leq \phi \leq 2\pi, \tag{4}$$

$$\hat{\mathbf{v}} = 0 \quad r \leq R,\ \theta = \frac{\pi}{2}, \quad 0 \leq \phi \leq 2\pi, \tag{5}$$

and, on the interface of the hemispherical bump ($r = R, 0 \leq \theta \leq \frac{\pi}{2}, 0 \leq \phi \leq 2\pi$), we have to match the inner and outer solutions by imposing (i) the kinetic condition for two phases, (ii) the continuity of the tangential velocity in two directions and (iii) the continuity of the shearing surface force per unit area in two directions. These boundary conditions are written in a general form:

$$\begin{aligned} &\boldsymbol{e}_r \cdot \mathbf{v} = \boldsymbol{e}_r \cdot \hat{\mathbf{v}} = 0, \\ &\boldsymbol{e}_r \times \mathbf{v} = \boldsymbol{e}_r \times \hat{\mathbf{v}}, \\ &\boldsymbol{e}_r \times \{\boldsymbol{\sigma} \cdot \boldsymbol{e}_r\} = \boldsymbol{e}_r \times \left\{\hat{\boldsymbol{\sigma}} \cdot \boldsymbol{e}_r\right\}, \end{aligned} \tag{6}$$

with $\boldsymbol{e}_r$ the radial normal unit vector at the bump surface.

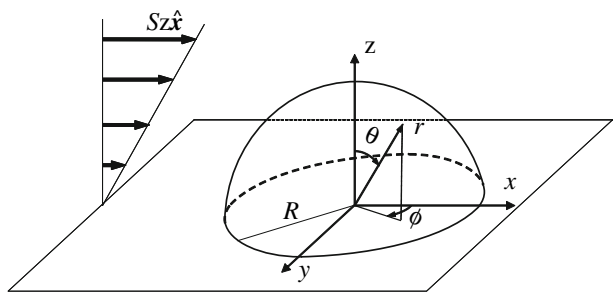

Fig. 1 Configuration for the problem

3 General solution

In the subsequent developments we will assume that all variables have been non-dimensionalized using S, ρ, η in the outer region and S, $\hat{\rho}$, $\hat{\eta}$ in the inner region together with a reference length scale given by the radius of the drop R. We will also introduce the disturbances of the velocity vectors $\mathbf{v}$ and $\hat{\mathbf{v}}$ from the linear shear flow as

$$\boldsymbol{q} = \boldsymbol{e}_x z - \mathbf{v}, \quad \hat{\boldsymbol{q}} = \boldsymbol{e}_x z - \hat{\mathbf{v}}. \tag{7}$$

These disturbances satisfy the continuity and Stokes equations:

$$\nabla \cdot \boldsymbol{q} = \nabla \cdot \hat{\boldsymbol{q}} = 0, \tag{8}$$

$$\nabla^2 \boldsymbol{q} = -\nabla p \quad \nabla^2 \hat{\boldsymbol{q}} = -\nabla \hat{p}. \tag{9}$$

The boundary conditions for no-slip walls are now expressed by

$$\boldsymbol{q} = 0 \quad r \geq 1, \ \theta = \frac{\pi}{2}, \ 0 \leq \phi \leq 2\pi, \tag{10}$$

$$\hat{\boldsymbol{q}} = 0 \quad r \leq 1, \ \theta = \frac{\pi}{2}, \ 0 \leq \phi \leq 2\pi, \tag{11}$$

while, considering the shear velocity $\boldsymbol{e}_x z$ written in spherical coordinates, we can rewrite the boundary conditions (6) using the disturbance velocities as

$$\begin{aligned} &q_r - \cos\theta \sin\theta \cos\phi = 0, \quad \hat{q}_r - \cos\theta \sin\theta \cos\phi = 0, \ q_\theta = \hat{q}_\theta, \quad q_\phi = \hat{q}_\phi, \\ &\frac{\partial q_\theta}{\partial r} - q_\theta = \lambda \left(\frac{\partial \hat{q}_\theta}{\partial r} - \hat{q}_\theta \right), \quad \frac{\partial q_\phi}{\partial r} - q_\phi = \lambda \left(\frac{\partial \hat{q}_\phi}{\partial r} - \hat{q}_\phi \right) \ r = 1, 0 \leq \theta \leq \pi/2, \ 0 \leq \phi \leq 2\pi. \end{aligned} \tag{12}$$

To reduce the ϕ-dependence of the boundary conditions (12) and obtain an axisymmetrical formulation of the problem, we introduce u, v, w, $\hat{u}$, $\hat{v}$, and $\hat{w}$ given by

$$u = \frac{q_r}{\cos\phi}, \quad v = \frac{q_\theta}{\cos\phi}, \quad w = \frac{q_\phi}{\sin\phi}, \quad \hat{u} = \frac{\hat{q}_r}{\cos\phi}, \quad \hat{v} = \frac{\hat{q}_\theta}{\cos\phi}, \quad \hat{w} = \frac{\hat{q}_\phi}{\sin\phi}.$$

We further introduce U, V, and W as functions of the velocity components u, v and w:

$$U = u \sin\theta + v \cos\theta + w, \quad V = u \sin\theta + v \cos\theta - w, \quad W = u \cos\theta - v \sin\theta,$$

and for the inner region, $\hat{U}$, $\hat{V}$ and $\hat{W}$ are similarly defined. Then, we may rewrite the boundary conditions on the droplet surface, using U, V, W, $\hat{U}$, $\hat{V}$ and $\hat{W}$ as

$$W \cos\theta + \left(\frac{U + V}{2} \right) \sin\theta - \cos\theta \sin\theta = 0, \tag{13}$$

$$\hat{W} \cos\theta + \left(\frac{\hat{U} + \hat{V}}{2} \right) \sin\theta - \cos\theta \sin\theta = 0, \tag{14}$$

$$-W \sin\theta + U \cos\theta = -\hat{W} \sin\theta + \hat{U} \cos\theta, \tag{15}$$

$$-W \sin\theta + V \cos\theta = -\hat{W} \sin\theta + \hat{V} \cos\theta, \tag{16}$$

$$\left(\frac{\partial}{\partial r} - 1 \right) (-W \sin\theta + U \cos\theta) = \lambda \left(\frac{\partial}{\partial r} - 1 \right) (-\hat{W} \sin\theta + \hat{U} \cos\theta), \tag{17}$$

$$\left(\frac{\partial}{\partial r} - 1 \right) (-W \sin\theta + V \cos\theta) = \lambda \left(\frac{\partial}{\partial r} - 1 \right) (-\hat{W} \sin\theta + \hat{V} \cos\theta). \tag{18}$$

As for the pressure field, we define P and $\hat{P}$ as

$$P = -\frac{p}{\cos\phi}, \quad \hat{P} = -\frac{\hat{p}}{\cos\phi}. \tag{19}$$

Since in the creeping-flow approximation the pressure is harmonic, we can give a non-divergent solution in a series of the associated Legendre functions P_n^m:

$$P = \sum_{n=1}^{\infty} \frac{A_n P_n^1(\mu)}{r^{n+1}}, \quad \hat{P} = \sum_{n=1}^{\infty} \hat{A}_n r^n P_n^1(\mu), \tag{20}$$

where $\mu = \cos\theta$ and A_n, $\hat{A}_n$ are unknown constants to be determined with the boundary conditions. Here we employ the definition of the associated Legendre functions defined in terms of the polynomials of zeroth order as $P_n^m(x) = (1-x^2)^{m/2}\mathrm{d}^m P_n(x)/\mathrm{d}x^m$ (e.g., $P_1^1(\cos\theta) = \sin\theta$). From the Stokes equations (9), we can determine the general solutions in the expansion form

$$W = \sum_{n=1}^{\infty} \frac{nA_n}{2(2n+1)r^n} P_{n+1}^1(\mu) + \sum_{n=2}^{\infty} \frac{C_n}{r^n} P_{n-1}^1(\mu),$$

$$U = \sum_{n=1}^{\infty} \frac{A_n}{2(2n+1)r^n} P_{n+1}^2(\mu) + \sum_{n=3}^{\infty} \frac{E_n}{r^n} P_{n-1}^2(\mu),$$

$$V = -\sum_{n=1}^{\infty} \frac{n(n+1)A_n}{2(2n+1)r^n} P_{n+1}(\mu) + \sum_{n=1}^{\infty} \frac{G_n}{r^n} P_{n-1}(\mu),$$

$$\hat{W} = \sum_{n=2}^{\infty} \frac{(n+1)\hat{A}_n r^{n+1}}{2(2n+1)} P_{n-1}^1(\mu) + \sum_{n=0}^{\infty} \hat{C}_n r^{n+1} P_{n+1}^1(\mu),$$

$$\hat{U} = -\sum_{n=3}^{\infty} \frac{\hat{A}_n r^{n+1}}{2(2n+1)} P_{n-1}^2(\mu) + \sum_{n=1}^{\infty} \hat{E}_n r^{n+1} P_{n+1}^2(\mu),$$

$$\hat{V} = \sum_{n=1}^{\infty} \frac{n(n+1)\hat{A}_n r^{n+1}}{2(2n+1)} P_{n-1}(\mu) + \sum_{n=0}^{\infty} \hat{G}_n r^{n+1} P_{n+1}(\mu),$$

with C_n, E_n, G_n and $\hat{C}_n$, $\hat{E}_n$, $\hat{G}_n$ being additional constants. Upon using the no-slip boundary condition on the plane wall (10)–(11) we get:

$$C_{2n} = \frac{2n+1}{2(4n+1)} A_{2n}, \quad E_{2n-1} = \frac{(2n+1)A_{2n-1}}{4(n-1)(4n-1)}, \quad G_{2n-1} = -\frac{(2n-1)^2 A_{2n-1}}{2(4n-1)}, \quad \hat{C}_{2n} = \frac{n\hat{A}_{2n}}{4n+1},$$

$$\hat{E}_{2n-1} = -\frac{(n-1)\hat{A}_{2n-1}}{(2n+1)(4n-1)}, \quad \hat{G}_{2n-1} = \frac{2n^2\hat{A}_{2n-1}}{4n-1},$$

and, imposing the continuity equation (8) together with (10)–(11), we find:

$$C_{2n-1} = \frac{(2n-1)(2n+1)}{4(4n-1)(n-1)} A_{2n-1}, \quad E_{2n} = \frac{1}{2(n-1)(2n-1)} \left\{ \frac{(2n-3)(2n+1)}{4n+1} A_{2n} + G_{2n} \right\},$$

$$\hat{C}_{2n-1} = \frac{2n(n-1)}{(2n+1)(4n-1)} \hat{A}_{2n-1}, \quad \hat{E}_{2n} = \frac{1}{2(n+1)(2n+3)} \left\{ -\frac{4n(n+2)}{4n+1} \hat{A}_{2n} + \hat{G}_{2n} \right\},$$

while, for the low-order coefficients, we obtain

$$A_1 = G_1 = \hat{E}_1 = \hat{C}_0 = \hat{C}_1 = 0,$$

and

$$\hat{A}_1 \neq 0, \quad \hat{G}_0 \neq 0.$$

Using all these recursion relations we can rewrite the general solutions for the outer ($\mathbf{v} = (v_r, v_\theta, v_\phi)$) and inner velocities ($\hat{\mathbf{v}} = (\hat{v}_r, \hat{v}_\theta, \hat{v}_\phi)$) representing the solution of the equation set (1)–(6):

$$v_r = \left\{ r\cos\theta\sin\theta - W\cos\theta - \left(\frac{U+V}{2}\right)\sin\theta \right\}\cos\phi, \tag{21}$$

$$v_\theta = \left\{ r\cos^2\theta + W\sin\theta - \left(\frac{U+V}{2}\right)\cos\theta \right\}\cos\phi, \tag{22}$$

$$v_\phi = \left(-r\cos\theta - \frac{U}{2} + \frac{V}{2} \right)\sin\phi, \tag{23}$$

$$\hat{v}_r = \left\{ r\cos\theta\sin\theta - \hat{W}\cos\theta - \left(\frac{\hat{U}+\hat{V}}{2}\right)\sin\theta \right\}\cos\phi, \tag{24}$$

$$\hat{v}_\theta = \left\{ r\cos^2\theta + \hat{W}\sin\theta - \left(\frac{\hat{U}+\hat{V}}{2}\right)\cos\theta \right\}\cos\phi, \tag{25}$$

$$\hat{v}_\phi = \left(-r\cos\theta - \frac{\hat{U}}{2} + \frac{\hat{V}}{2} \right)\sin\phi, \tag{26}$$

where

$$W = \frac{3A_2P_1^1(\mu)}{10r^2} + \frac{15A_3P_2^1(\mu)}{28r^3} + \sum_{n=2}^{\infty}\left[\left(\frac{(n-1)A_{2n-2}}{(4n-3)r^{2n-2}} + \frac{(2n+1)A_{2n}}{2(4n+1)r^{2n}} \right) P_{2n-1}^1(\mu) + \left(\frac{(2n-1)A_{2n-1}}{2(4n-1)r^{2n-1}} + \frac{(2n+1)(2n+3)A_{2n+1}}{4n(4n+3)r^{2n+1}} \right) P_{2n}^1(\mu) \right], \tag{27}$$

$$U = \frac{5A_3P_2^2(\mu)}{28r^3} + \sum_{n=2}^{\infty}\left[\left(\frac{A_{2n-2}}{2(4n-3)r^{2n-2}} + \frac{(2n-3)(2n+1)A_{2n}}{2(n-1)(2n-1)(4n+1)r^{2n}} + \frac{G_{2n}}{2(n-1)(2n-1)r^{2n}} \right) P_{2n-1}^2(\mu) + \left(\frac{A_{2n-1}}{2(4n-1)r^{2n-1}} + \frac{(2n+3)A_{2n+1}}{4n(4n+3)r^{2n+1}} \right) P_{2n}^2(\mu) \right], \tag{28}$$

$$V = \frac{G_2P_1(\mu)}{r^2} - \frac{9A_3P_2(\mu)}{14r^3} + \sum_{n=2}^{\infty}\left[\left(-\frac{(n-1)(2n-1)A_{2n-2}}{(4n-3)r^{2n-2}} + \frac{G_{2n}}{r^{2n}} \right) P_{2n-1}(\mu) + \left(-\frac{n(2n-1)A_{2n-1}}{(4n-1)r^{2n-1}} - \frac{(2n+1)^2A_{2n+1}}{2(4n+3)r^{2n+1}} \right) P_{2n}(\mu) \right], \tag{29}$$

$$\hat{W} = \frac{3\hat{A}_2r^3P_1^1(\mu)}{10} + \sum_{n=2}^{\infty}\left(\frac{(2n+1)\hat{A}_{2n}r^{2n+1}}{2(4n+1)} + \frac{(n-1)\hat{A}_{2n-2}r^{2n-1}}{4n-3} \right) P_{2n-1}^1(\mu) + \sum_{n=1}^{\infty}\left(\frac{(n+1)\hat{A}_{2n+1}r^{2n+2}}{4n+3} + \frac{2n(n-1)\hat{A}_{2n-1}r^{2n}}{(2n+1)(4n-1)} \right) P_{2n}^1(\mu), \tag{30}$$

$$\hat{U} = \sum_{n=2}^{\infty}\left(-\frac{\hat{A}_{2n}r^{2n+1}}{2(4n+1)} - \frac{2(n-1)(n+1)\hat{A}_{2n-2}r^{2n-1}}{n(2n+1)(4n-3)} + \frac{\hat{G}_{2n-2}r^{2n-1}}{2n(2n+1)} \right) P_{2n-1}^2(\mu) + \sum_{n=1}^{\infty}\left(-\frac{\hat{A}_{2n+1}r^{2n+2}}{2(4n+3)} - \frac{(n-1)\hat{A}_{2n-1}r^{2n}}{(2n+1)(4n-1)} \right) P_{2n}^2(\mu), \tag{31}$$

Table 1 Coefficients for $\lambda = 0$

n	A_{2n+1}	A_{2n}	G_{2n}	$\hat{A}_{2n-1}$	$\hat{A}_{2n}$	$\hat{G}_{2n-2}$
1	-4.2435×10^{-12}	0.66667	0.40000	−11.47649	2.53882	8.03099
2	-2.3846×10^{-12}	-9.0339×10^{-14}	-2.5928×10^{-13}	−2.13519	0.17201	5.42824
3	1.1579×10^{-12}	-1.8727×10^{-14}	2.8944×10^{-13}	0.24983	−0.071796	0.12475
4	-1.8929×10^{-12}	-7.2444×10^{-14}	-1.8123×10^{-13}	−0.062825	0.036175	−0.082789
5	-2.1743×10^{-13}	1.6780×10^{-14}	2.5391×10^{-13}	0.019726	−0.020377	0.056309
6	-2.7782×10^{-13}	-1.5622×10^{-14}	-2.1449×10^{-13}	−0.0063530	0.012379	−0.039535
7	3.3070×10^{-15}	1.3030×10^{-14}	1.6910×10^{-13}	0.0015681	−0.0079442	0.028544
8	-8.3398×10^{-14}	4.3793×10^{-15}	-2.0627×10^{-13}	0.00024267	0.0053167	−0.021091
9	-7.9357×10^{-15}	3.6435×10^{-14}	9.0663×10^{-14}	−0.00090699	−0.0036784	0.015882
10	-1.8344×10^{-13}	-1.1164×10^{-14}	-1.4936×10^{-13}	0.0011024	0.0026142	−0.012147
11	1.7744×10^{-14}	1.6463×10^{-14}	1.3542×10^{-13}	−0.0011030	−0.0018995	0.0094079
12	-3.0430×10^{-13}	6.7278×10^{-15}	-2.5442×10^{-13}	0.0010260	0.0014061	−0.0073615
13	-2.2858×10^{-13}	1.5070×10^{-14}	7.3790×10^{-14}	−0.00092290	−0.0010573	0.0058075
14	-2.6355×10^{-13}	-1.8224×10^{-14}	-5.9443×10^{-14}	0.00081663	0.00080565	−0.0046107
15	2.3231×10^{-13}	-1.0819×10^{-14}	2.0463×10^{-13}	−0.00071683	−0.00062094	0.0036777

$$\hat{V} = \frac{\hat{A}_1 r^2 P_0(\mu)}{3} + \sum_{n=1}^{\infty} \left[\left(\frac{n(2n+1)\hat{A}_{2n} r^{2n+1}}{4n+1} + \hat{G}_{2n-2} r^{2n-1} \right) P_{2n-1}(\mu) + \left(\frac{(n+1)(2n+1)\hat{A}_{2n+1} r^{2n+2}}{4n+3} + \frac{2n^2 \hat{A}_{2n-1} r^{2n}}{4n-1} \right) P_{2n}(\mu) \right]. \tag{32}$$

In the previous expressions the six unknown sets of coefficients A_{2n+1}, A_{2n}, G_{2n}, $\hat{A}_{2n-1}$, $\hat{A}_{2n}$ and $\hat{G}_{2n-2}$ with $n \geq 1$ have now to be determined by the imposition of the six conditions (13)–(18) on the hemispherical bump.

3.1 Determination of the coefficients

To determine the coefficients A_{2n+1}, A_{2n}, G_{2n}, $\hat{A}_{2n-1}$, $\hat{A}_{2n}$ and $\hat{G}_{2n-2}$ for $n \geq 1$, we need recurrence formulae that can be deduced from the boundary conditions at $r = 1$ given by (13)–(18). These recurrence formulae are given in the appendix and, although they are written as infinite series, we numerically solve the problem by truncating the system of equations determining the coefficients. For each of the six coefficients we consider modes up to $n = 100$ and to have a good indication of the accuracy of this procedure, the numerically estimated coefficients are substituted in (13)–(18) until the boundary conditions are satisfied to at least five decimal places. The coefficients A_{2n+1}, A_{2n}, G_{2n}, $\hat{A}_{2n-1}$, $\hat{A}_{2n}$ and $\hat{G}_{2n-2}$ up to $n = 15$ are listed in Tables 1–4 for $\lambda = 0$, 0.1, 1, 10 and 10^{100} and to obtain the full solutions, they must be used in the equations (21)–(32).[1]

In Fig. 2 we show the kinematical structure of the flow and the development of stagnation points and flow reversal. Let us notice that for high viscosity ratio the streamlines plot is consistent with the results obtained by Pozrikidis [8].

It is now useful to check the validity for the two extreme limits $\lambda \to 0$ and $\lambda \to \infty$. For the free-slip bump, $\lambda = 0$, as is also confirmed by our numerical solution shown in Table 1 the solution is analytical and can be expressed as

$$A_n = \frac{2}{3}\delta_{n2}, \quad G_n = \frac{2}{5}\delta_{n2}.$$

Using this solution, we determine U, V, W and P

$$W = \frac{\sqrt{1-\mu^2}\mu^2}{r^2}, \quad U = \frac{(1-\mu^2)\mu}{r^2}, \quad V = \frac{(1-\mu^2)\mu}{r^2}, \quad P = \frac{2\sqrt{1-\mu^2}\mu}{r^3}.$$

[1] For the numerical coefficients corresponding to other values of λ the interested reader can contact the authors.

Table 2 Coefficients for $\lambda = 0.1$

n	A_{2n+1}	A_{2n}	G_{2n}	$\hat{A}_{2n-1}$	$\hat{A}_{2n}$	$\hat{G}_{2n-2}$
1	−0.17436	0.84972	0.50983	−10.46143	2.31835	7.49147
2	−0.077633	0.15800	−0.077149	−1.94082	0.15400	4.92646
3	0.012187	0.0094929	−0.0011555	0.22749	−0.064461	0.11746
4	−0.0035702	−0.0046015	0.0023703	−0.057379	0.032545	−0.077592
5	0.0012341	0.0025121	−0.0022646	0.018100	−0.018362	0.052686
6	−0.00042666	−0.0014877	0.0019020	−0.0058827	0.011167	−0.036976
7	0.00011347	0.00093504	−0.0015382	0.0014964	−0.0071731	0.026705
8	0.000013522	−0.00061510	0.0012302	0.00017241	0.0048045	−0.019748
9	−0.000063680	0.00041948	−0.00098250	−0.00079079	−0.0033262	0.014888
10	0.000080443	−0.00029453	0.00078655	0.00097802	0.0023654	−0.011407
11	−0.000082443	0.00021183	−0.00063199	−0.00098504	−0.0017197	0.0088482
12	0.000078085	−0.00015543	0.00050977	0.00091948	0.0012736	−0.0069382
13	−0.000071276	0.00011601	−0.00041261	−0.00082899	−0.00095812	0.0054870
14	0.000063845	−0.000087837	0.00033493	0.00073472	0.00073043	−0.0043687
15	−0.000056630	0.000067335	−0.00027242	−0.00064571	−0.00056322	0.0034961

Table 3 Coefficients for $\lambda = 1$

n	A_{2n+1}	A_{2n}	G_{2n}	$\hat{A}_{2n-1}$	$\hat{A}_{2n}$	$\hat{G}_{2n-2}$
1	−0.97542	1.68344	1.01007	−5.85249	1.31294	5.05033
2	−0.42739	0.87935	−0.40999	−1.06849	0.077130	2.67984
3	0.067950	0.048954	−0.014276	0.12684	−0.033073	0.077672
4	−0.020266	−0.024073	0.017863	−0.032570	0.016955	−0.049837
5	0.0071884	0.013276	−0.015674	0.010543	−0.0096669	0.033457
6	−0.0026054	−0.0079212	0.012751	−0.0035922	0.0059251	−0.023387
7	0.00079580	0.0050080	−0.010168	0.0010494	−0.0038295	0.016889
8	−0.000042750	−0.0033104	0.0080860	−0.000054498	0.0025779	−0.012520
9	−0.00026832	0.0022669	−0.0064524	−0.00033322	−0.0017925	0.0094793
10	0.00038388	−0.0015974	0.0051775	0.00046672	0.0012795	−0.0073022
11	−0.00041078	0.0011527	−0.0041798	−0.00049081	−0.00093345	0.0057059
12	0.00039788	−0.00084839	0.0033941	0.00046853	0.00069351	−0.0045116
13	−0.00036830	0.00063500	−0.0027709	−0.00042837	−0.00052328	0.0036025
14	0.00033312	−0.00048214	0.0022727	0.00038336	0.00040007	−0.0029001
15	−0.00029762	0.00037060	−0.0018715	−0.00033936	−0.00030935	0.0023503

Table 4 Coefficients for $\lambda = 10$

n	A_{2n+1}	A_{2n}	G_{2n}	$\hat{A}_{2n-1}$	$\hat{A}_{2n}$	$\hat{G}_{2n-2}$
1	−1.83516	2.55162	1.53097	−1.10110	0.25418	2.56548
2	−0.78449	1.64184	−0.68804	−0.19612	0.011796	0.47557
3	0.12819	0.079556	−0.050045	0.023929	−0.0054338	0.018141
4	−0.039327	−0.040886	0.045731	−0.0063205	0.0028862	−0.011069
5	0.014454	0.023098	−0.036923	0.0021199	−0.0016810	0.0072831
6	−0.0055521	−0.013997	0.029024	−0.00076551	0.0010455	−0.0050478
7	0.0019496	0.0089486	−0.022775	0.00025708	−0.00068302	0.0036351
8	−0.00039965	−0.0059665	0.017979	−0.000050954	0.00046375	−0.0026961
9	−0.00027530	0.0041147	−0.014313	−0.000034189	−0.00032475	0.0020468
10	0.00055414	−0.0029172	0.011495	0.000067373	0.00023324	−0.0015835
11	−0.00064763	0.0021163	−0.0093099	−0.000077380	−0.00017109	0.0012443
12	0.00065388	−0.0015652	0.0075980	0.000076998	0.00012775	−0.00099055
13	−0.00062032	0.0011769	−0.0062438	−0.000072149	−0.000096843	0.00079718
14	0.00057041	−0.00089748	0.0051623	0.000065643	0.000074373	−0.00064750
15	−0.00051578	0.00069277	−0.0042910	−0.000058812	−0.000057759	0.00053005

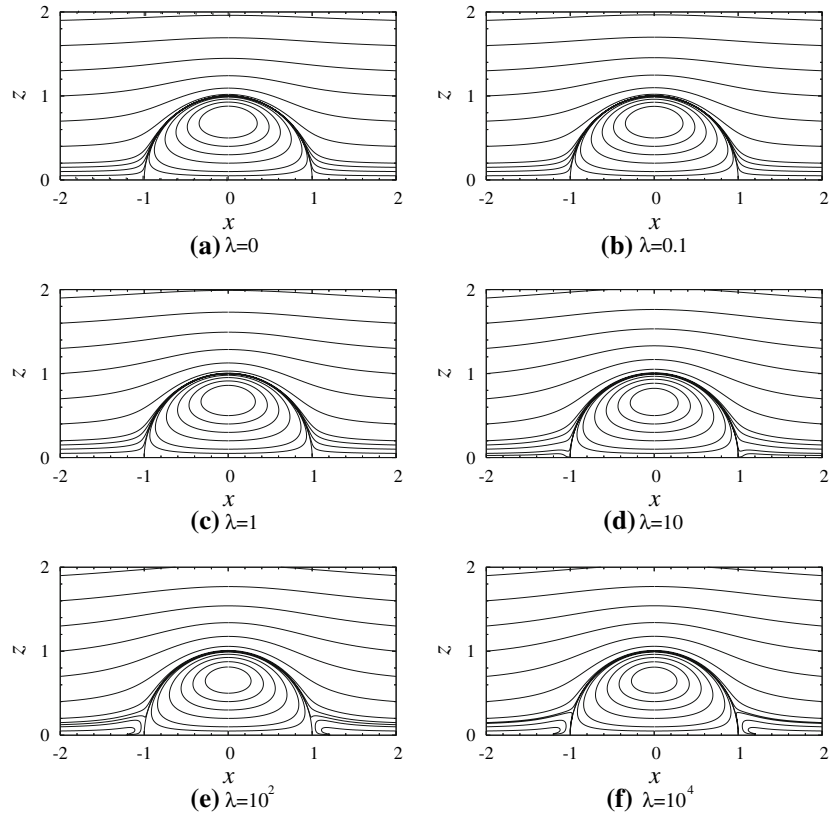

Fig. 2 Streamline patterns in the in xz-mid-plane (for $y = 0$)

The velocity field around the hemisphere is then given by

$$\mathbf{v} = \boldsymbol{e}_r \left(r - \frac{1}{r^2} \right) \cos\theta \sin\theta \cos\phi + \boldsymbol{e}_\theta r \cos^2\theta \cos\phi - \boldsymbol{e}_\phi r \cos\theta \sin\phi$$

which can also be rewritten together with the pressure in Cartesian coordinates

$$\mathbf{v} = \boldsymbol{e}_x \left(z - \frac{x^2 z}{r^5} \right) - \boldsymbol{e}_y \frac{xyz}{r^5} - \boldsymbol{e}_z \frac{xz^2}{r^5}, \quad p = -\frac{2xz}{r^5}. \tag{33}$$

It should be noted that the present solution (33) is same as that representing the flow around a free-slip sphere in an infinite fluid. This is because the presence of the free-slip sphere does not alter the θ- and ϕ-components of the velocity vector from the uniform shear flow and then the modulated velocity becomes zero at $z = 0$.

In the case of the largest viscosity ratio $\lambda = 10^{100}$, the coefficients A_{2n+1}, A_{2n} and G_{2n} listed in Table 5 show quantitative agreement with those for the no-slip bump shown in the paper by Price [7]. The inner solution is analytical and given by $\hat{A}_n = 0$ and $\hat{G}_n = 2\delta_{0n}$ which implies a zero velocity inside the bump.

3.2 Torque and force

We now evaluate the force and the torque acting on the hemisphere for various viscosity ratios. The general strategy will be to write them as functions of the constants A_{2n}, S_{2n+1}, G_{2n} and then use the coefficients obtained from the numerical solution in the previous section in order to evaluate them. To do this, we write the force $\boldsymbol{F}$ and the torque $\boldsymbol{T}$ in the most general form

$$\boldsymbol{F} = \int_0^{2\pi} \mathrm{d}\phi \int_0^{\pi/2} \mathrm{d}\theta \ \sin\theta \ (\boldsymbol{\sigma} \cdot \boldsymbol{e}_r)_{r=1}, \quad \boldsymbol{T} = \int_0^{2\pi} \mathrm{d}\phi \int_0^{\pi/2} \mathrm{d}\theta \ \sin\theta \ [r\boldsymbol{e}_r \times (\boldsymbol{\sigma} \cdot \boldsymbol{e}_r)]_{r=1}.$$

Table 5 Coefficients for $\lambda = 10^{100}$

n	A_{2n+1}	A_{2n}	G_{2n}	$\hat{A}_{2n-1}$	$\hat{A}_{2n}$	$\hat{G}_{2n-2}$
1	−2.04530	2.75543	1.65326	-1.2272×10^{-99}	2.8662×10^{-100}	2.00000
2	−0.86783	1.82575	−0.73104	-2.1696×10^{-100}	1.2213×10^{-101}	5.1794×10^{-100}
3	0.14321	0.084338	−0.063687	2.6733×10^{-101}	-5.8109×10^{-102}	2.1417×10^{-101}
4	−0.044300	−0.044198	0.054743	-7.1196×10^{-102}	3.1280×10^{-102}	-1.2864×10^{-101}
5	0.016436	0.025196	−0.043364	2.4106×10^{-102}	-1.8352×10^{-102}	8.4124×10^{-102}
6	−0.0064047	−0.015350	0.033811	-8.8306×10^{-103}	1.1467×10^{-102}	-5.8150×10^{-102}
7	0.0023185	0.0098491	−0.026427	3.0574×10^{-103}	-7.5171×10^{-103}	4.1832×10^{-102}
8	−0.00054568	−0.0065846	0.020824	-6.9572×10^{-104}	5.1171×10^{-103}	-3.1021×10^{-102}
9	−0.00023620	0.0045508	−0.016566	-2.9333×10^{-104}	-3.5909×10^{-103}	2.3560×10^{-102}
10	0.00056676	−0.0032322	0.013305	6.8908×10^{-104}	2.5837×10^{-103}	-1.8242×10^{-102}
11	−0.00068450	0.0023485	−0.010782	-8.1786×10^{-104}	-1.8982×10^{-103}	1.4350×10^{-102}
12	0.00070095	−0.0017395	0.0088074	8.2541×10^{-104}	1.4194×10^{-103}	-1.1439×10^{-102}
13	−0.00067033	0.0013096	−0.0072468	-7.7965×10^{-104}	-1.0775×10^{-103}	9.2200×10^{-103}
14	0.00061962	−0.00099993	0.0060008	7.1306×10^{-104}	8.2854×10^{-104}	-7.5021×10^{-103}
15	−0.00056237	0.00077279	−0.0049970	-6.4124×10^{-104}	-6.4425×10^{-104}	6.1534×10^{-103}

Let us notice that the symmetry of the system with respect to ϕ is such that only the x-component of the planar force vector (F_x, F_y) and the y-component of the torque vector T_y are non-zero. To estimate these components, considering the kinetic condition in (12) and using U, V and W given by the general solution, we can exactly express the torque and force as functions of A_{2n},A_{2n+1} and G_{2n}:

$$F_x = \pi \left[\frac{1}{2} + \frac{4}{5} A_3 - \sum_{n=1}^{\infty} \frac{(-1)^n (2n+1)!!}{(2n-3)(2n-1)(2n-2)!!} \left(\frac{(4n^3 - 9n - 2) A_{2n}}{2(n+1)(4n+1)} + \frac{(2n^2 - 3n - 1) G_{2n}}{n(2n+1)} \right) \right], \tag{34}$$

$$T_y = \pi \left[-\frac{3}{5} A_2 + G_2 + \sum_{n=1}^{\infty} \frac{(-1)^n (2n+1)!!}{(2n-1)(2n)!!} A_{2n+1} \right], \tag{35}$$

with

$$(2n+1)!! = (2n+1) \times (2n-1) \times \cdots \times 1,$$
$$(2n)!! = (2n) \times (2n-2) \times \cdots \times 2, \quad 0!! = 1.$$

In the limit of a highly viscous droplet ($\lambda \to \infty$), from the numerical evaluation of the coefficients for $\lambda = 10^{100}$ (see Table 5), we determine the force and torque as

$$F_x = 4.30322\pi, \quad T_y = 2.44132\pi,$$

and both results are consistent with the evaluations $F_x = 4.30\pi$, $T_y = 2.44\pi$ for the rigid no-slip bump given in the paper by Price [7].

The profiles of F_x and T_y as functions of λ are, respectively, shown in Figs. 3 and 4. As is clearly shown, both the torque and the force approach a finite value for very small ($\lambda \to 0$) and large ($\lambda \to \infty$) viscosity ratios. Considering these asymptotic behaviors, we can estimate

$$\frac{F_x}{\pi} \approx \frac{2 + 4.51003\lambda}{1 + 1.04806\lambda}, \tag{36}$$

$$\frac{T_y}{\pi} \approx \frac{2.18808\lambda}{1 + 0.896271\lambda}, \tag{37}$$

in which the numerical coefficients have been determined from the method of least squares.

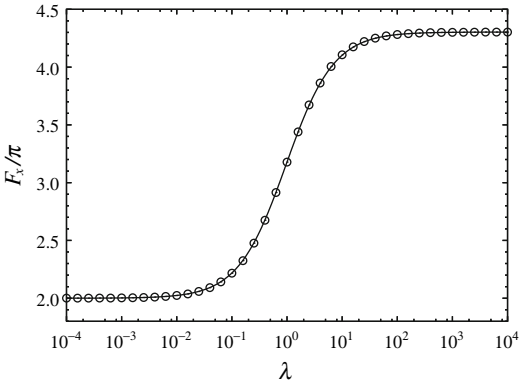

Fig. 3 The force acting on the hemisphere versus the viscosity ratio. The symbol ∘ corresponds to the evaluation based on (34). The solid line corresponds to the approximation (36)

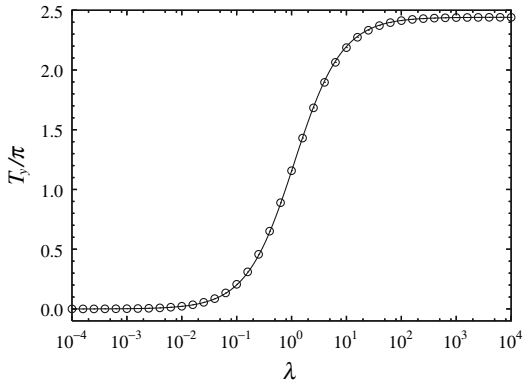

Fig. 4 The torque acting on the hemisphere versus the viscosity ratio. The symbol ∘ corresponds to the evaluation based on (35). The solid line corresponds to the approximation (37)

3.3 Effects of capillary number on deformation

In this section we study the local difference of the normal stress between the inner and outer regions of the bump. If we assume a finite surface tension γ at the droplet surface, the difference between the the two normal stresses must equal the surface tension times the local curvature of the hemispherical bump. In other words, for fixed surface tension, this gives the possibility to estimate the deformations on the droplet surface consistently with the Laplace law [18,19]. Based on the assumption that these deformations are small, we can introduce a capillary number as

$$\mathrm{Ca} = \frac{\eta S R_0}{\gamma},$$

where R_0, S and γ are dimensional length, shear and surface-tension scales. Next we write a dimensional stress tensor as

$$\boldsymbol{\sigma}^{(\mathrm{dim})} = \boldsymbol{\sigma} S\eta - P_s,$$

$$\hat{\boldsymbol{\sigma}}^{(\mathrm{dim})} = \hat{\boldsymbol{\sigma}} S\eta\lambda - \hat{P}_s,$$

where the contributions $\boldsymbol{\sigma}$ and $\hat{\boldsymbol{\sigma}}$ are purely dimensionless, i.e., they correspond to a unitary shear S and unitary viscosity η described in the previous sections. The terms P_s and $\hat{P}_s$ represent constant dimensional background pressures, i.e. the pressure inside/outside the bump in absence of flow. Assuming $\mathrm{Ca} \ll 1$, if we indicate with $r = R$ the position of the interface, we must write:

$$R(\theta, \phi) = R_0(1 + \mathrm{Ca}R^{(1)}(\theta, \phi) + \mathcal{O}(\mathrm{Ca}^2)), \tag{38}$$

where $R^{(1)}$ accounts for the displacement from the pure hemisphere. The Laplace law on the interface is written in a general form

$$\kappa^{(\mathrm{dim})}\gamma = \sigma_{rr}^{(\mathrm{dim})} - \hat{\sigma}_{rr}^{(\mathrm{dim})},$$

where $\kappa^{(\mathrm{dim})} = \kappa/R_0$ denotes the dimensional curvature, κ being its dimensionless counterpart. If $\mathrm{Ca} \ll 1$, the displacement is small enough and the curvature on the bump interface is given by

$$\begin{aligned}
\kappa &= R_0 \left\{ \nabla \cdot \left(\frac{\nabla(r-R)}{|\nabla(r-R)|} \right) \right\}_{r=R} \approx R_0 \left\{ \nabla^2 (r-R) \right\}_{r=R} \\
&= \frac{2}{1 + \mathrm{Ca}R^{(1)} + \cdots} - \left[\frac{1}{\sin\theta} \frac{\partial}{\partial\theta} \left(\sin\theta \frac{\partial}{\partial\theta} \right) + \frac{1}{\sin^2\theta} \frac{\partial^2}{\partial\phi^2} \right] \mathrm{Ca}R^{(1)} + \cdots \\
&= 2\mathrm{Ca}^0 - \mathrm{Ca}^1 \left[2 + \frac{1}{\sin\theta} \frac{\partial}{\partial\theta} \left(\sin\theta \frac{\partial}{\partial\theta} \right) + \frac{1}{\sin^2\theta} \frac{\partial^2}{\partial\phi^2} \right] R^{(1)} + \mathcal{O}(\mathrm{Ca}^2),
\end{aligned}$$

hence $\kappa/\mathrm{Ca} = \left(\sigma_{rr} - \lambda\hat{\sigma}_{rr}\right)_{r=1} + (\hat{P}_s - P_s)/(S\eta)$ and

$$\frac{2}{\mathrm{Ca}} - \left[2 + \frac{1}{\sin\theta}\frac{\partial}{\partial\theta}\left(\sin\theta\frac{\partial}{\partial\theta}\right) + \frac{1}{\sin^2\theta}\frac{\partial^2}{\partial\phi^2}\right] R^{(1)} + \mathcal{O}(\mathrm{Ca}^1) = \left(\sigma_{rr} - \lambda\hat{\sigma}_{rr}\right)_{r=1} + (\hat{P}_s - P_s)/(S\eta). \tag{39}$$

In the absence of the shear flow, the pressure is constant inside and outside the bump and equal to $\hat{P}_s$ and P_s, respectively. The gap between the two pressures is determined by $(\hat{P}_s - P_s)/(S\eta) = 2\mathrm{Ca}^{-1}$ from the $\mathcal{O}(\mathrm{Ca}^{-1})$ of (39). This means that, in presence of a non-zero velocity, in order to find consistency with the Laplace law, we should consider a finite displacement given by a non-zero $R^{(1)}$ in (38). To determine this displacement, Eq. 39 is solved at $\mathcal{O}(\mathrm{Ca}^0)$:

$$-\left[2 + \frac{1}{\sin\theta}\frac{\partial}{\partial\theta}\left(\sin\theta\frac{\partial}{\partial\theta}\right) + \frac{1}{\sin^2\theta}\frac{\partial^2}{\partial\phi^2}\right] R^{(1)} = \left(\sigma_{rr} - \lambda\hat{\sigma}_{rr}\right)_{r=1}, \tag{40}$$

with the boundary condition

$$R^{(1)} = 0 \quad \text{at } \theta = \frac{\pi}{2}, \ \ 0 \le \phi \le 2\pi. \tag{41}$$

This condition fixes the contact line, while accounting for the shape deformation of the droplet. More generally, the contact line will be deformed and, in principle, one can solve for the contact-line shape as part of the problem [12,13]. However, the requirement (41) is still useful, given the comparison it allows with other works [14,15].

If we write the normal stress jump in the expansion form with respect to the associated Legendre polynomials

$$\left(\sigma_{rr} - \lambda\hat{\sigma}_{rr}\right)_{r=1} = \sum_{n=1}^{\infty} Q_n P_n^1(\mu)\cos\phi,$$

the expansion coefficients Q_n can be determined as:

$$\begin{aligned} Q_{2n} = {} & \frac{2\delta_{1n}}{3}(1-\lambda) + \frac{4n^2+6n-1}{4n-1}A_{2n} + \frac{2(n+1)^2(2n+3)(8n^2+6n-3)}{n(2n+1)(4n+3)(4n+5)}A_{2n+2} + \frac{2(n+1)}{n(2n+1)}G_{2n+2} \\ & + \lambda\left(\frac{2(n-1)(2n-1)^2(4n^2+n-2)}{n(2n+1)(4n-3)(4n-1)}\hat{A}_{2n-2} + \frac{4n^2-2n-3}{4n+3}\hat{A}_{2n} + \frac{2n-1}{n(2n+1)}\hat{G}_{2n-2}\right), \end{aligned} \tag{42}$$

$$\begin{aligned} Q_{2n-1} = {} & \frac{4n^2+2n-3}{4n-3}A_{2n-1} + \frac{(n+1)(2n+1)^2}{n(4n+1)}A_{2n+1} \\ & + \lambda\left(\frac{4(n-1)^2(2n-3)}{(2n-1)(4n-3)}\hat{A}_{2n-3} + \frac{4n^2-6n-1}{4n+1}\hat{A}_{2n-1}\right). \end{aligned} \tag{43}$$

We now solve (40) and determine the displacement

$$R^{(1)} = \left(\frac{R_0^{(1)}\sqrt{1-\mu^2}}{1+\mu} + \sum_{n=2}^{\infty} R_n^{(1)} P_n^1(\mu)\right)\cos\phi, \tag{44}$$

where

$$R_0^{(1)} = \sum_{k=2}^{\infty} \frac{(-1)^k(2k-1)!!}{2(k-1)(2k+1)(2k-2)!!} Q_{2k-1}, \tag{45}$$

$$R_n^{(1)} = \frac{Q_n}{(n-1)(n+2)} \quad \text{for} \quad n \ge 2. \tag{46}$$

Concerning the ϕ-dependence of the normal-stress jump, this is simply proportional to $\cos\phi$. In Fig. 5 we show the deformation of the bump on the plane of $y = 0$ with a capillary number $\mathrm{Ca} = 0.05$. These deformations have been estimated from (44), (45) and (46) with the numerical coefficients in (42) and (43) determined with the procedure of the previous section. Moreover, to better quantify the role of deformations with respect to the hemispherical

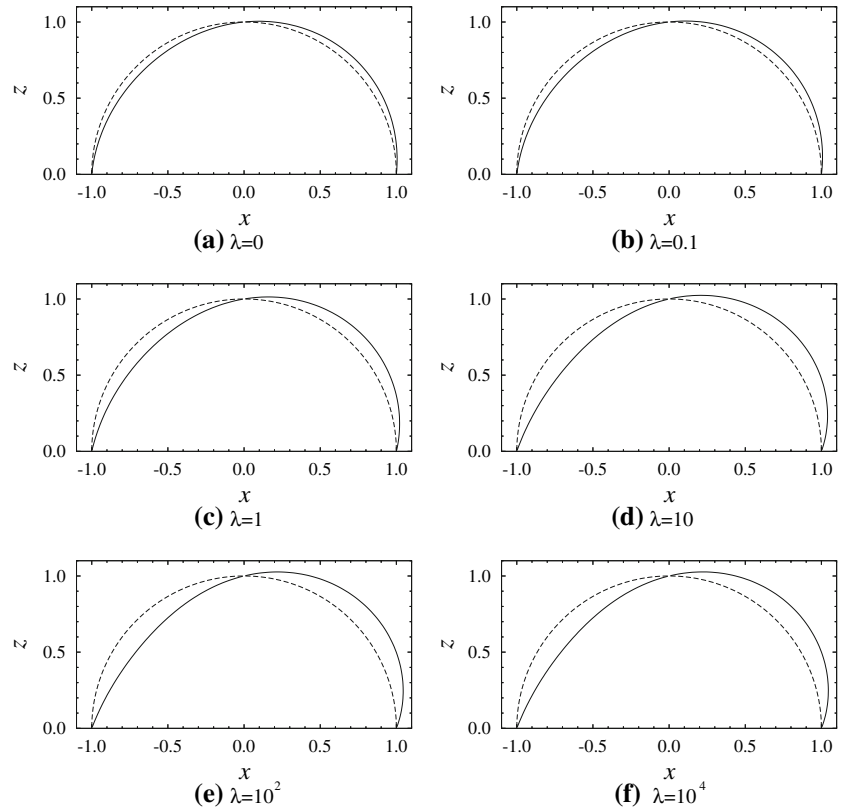

Fig. 5 Shape of the bump on the plane of $y = 0$ for various viscosity ratios λ. The dashed line shows the hemisphere with no deformation. The solid line shows the deformed interface for a capillary number $\mathrm{Ca} = 0.05$

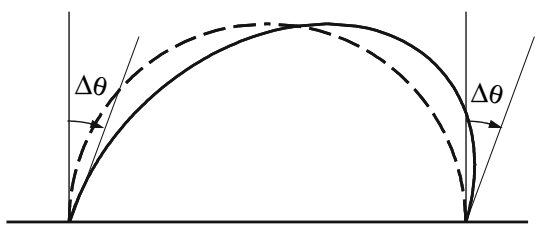

Fig. 6 Advancing and receding contact angles due to deformations are introduced in the problem in the small-capillary-number regime

bump, advancing and receding contact angles should be, respectively, defined by $\pi/2 + \Delta\theta$ and $\pi/2 - \Delta\theta$, with $\Delta\theta$ proportional to Ca if the deformation is small enough (see Fig. 6).

For various viscosity ratios λ, $\Delta\theta/\mathrm{Ca}$ is then plotted in Fig. 7. Considering the asymptotic behaviors, this deformation can be approximated by

$$\Delta\theta \approx \frac{(2 + 7.07185\lambda)}{(1 + 0.908826\lambda)}\mathrm{Ca}, \tag{47}$$

in which the numerical coefficients have been determined from the method of least squares.

For the case of a hemispherical droplet whose viscosity is equal to the surrounding fluid ($\lambda = 1$), it is instructive to compare our results with those of Li and Pozrikidis [14].

In Fig. 8 we plot the deformation parameter $D = (A - B)/(A + B)$ as a function of the capillary number. A and B are, respectively, the maximum and minimum radial distances of the interface from the origin. Note that the corresponding slope for a spherical drop suspended in an infinite simple shear flow is equal to 35/32 [20] and suggests that the wall promotes the deformation of the drop which is also confirmed by the computation of Li and

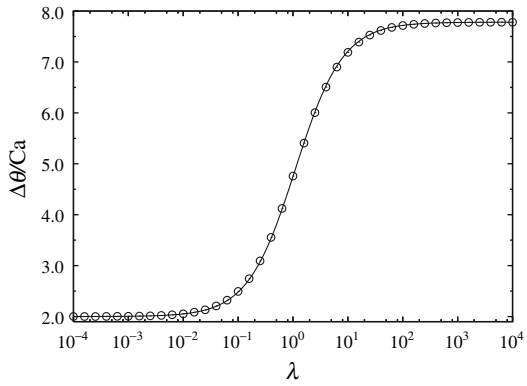

Fig. 7 Contact angle deformations as a function of the viscosity ratio in the limit of small capillary numbers. The symbol ∘ corresponds to the solution based on (40). The solid line corresponds to the approximation (47)

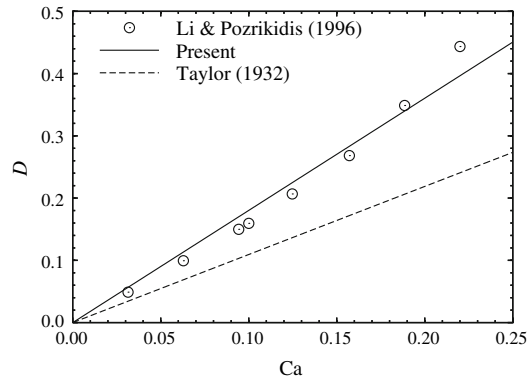

Fig. 8 Deformation parameter D as a function of the capillary number for a viscosity ratio $\lambda = 1$. Our solution (*straight line*) is compared with the results obtained with the boundary-integral method (∘) by Li and Pozrikidis [14]. The deformation parameter for the case of a droplet suspended in an infinite shear flow is also reported (*dashed line*)

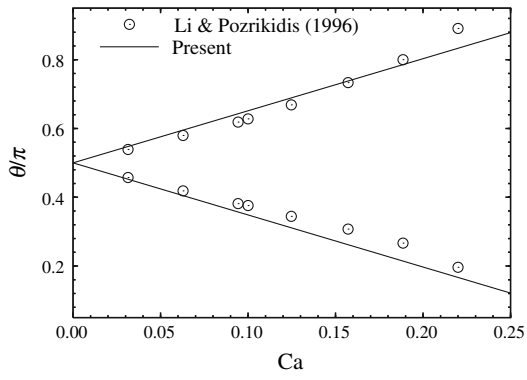

Fig. 9 Advancing and receding contact angles as a function of the capillary number for a viscosity ratio $\lambda = 1$. Our results (*straight line*) are compared with the numerical results obtained with the boundary integral method (∘) by Li and Pozrikidis [14]

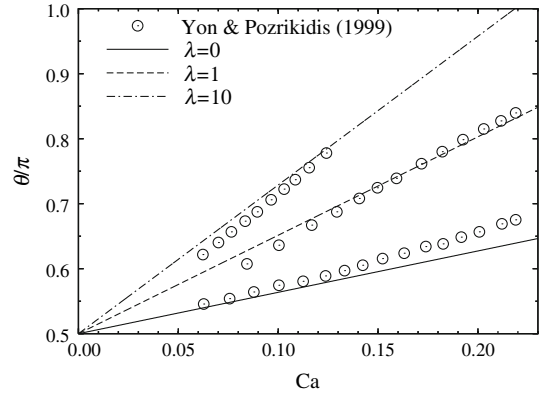

Fig. 10 Advancing contact angles as a function of the capillary number for viscosity ratios $\lambda = 0, 1, 10$. Our results are compared with the numerical results obtained with the boundary integral method (∘) by Yon and Pozrikidis [15]

Pozrikidis [14] (see their Fig. 6(e)) with the boundary-integral method. To further compare our results with those of Li and Pozrikidis, in Fig. 9 we plot the advancing and receding contact angles as functions of the capillary number and a good agreement is found.

The numerical investigations of Li and Pozrikidis [14] were also extended in another paper by Yon and Pozrikidis [15] which examined the role played by the viscosity ratio. In particular in Fig. 10 we compare our result for the advancing contact angle as a function of the capillary number with the numerical results shown in Fig. 3(g) of the paper by Yon and Pozrikidis and quantitative agreement is found.

4 Concluding remarks

An exact solution for the problem of a linear shear flow overpassing a hemispherical droplet resting on a plane wall has been computed explicitly. The results presented here are the natural generalization of the ones proposed in an

earlier paper by Price [7] who investigated the case of a hemispherical no-slip bump. Several expressions, including the torque and force acting on the hemisphere, have been derived exactly and computed as a function of the viscosity ratio. The small deformations on the hemispherical surface have also been quantified in the limit of small capillary numbers and a comparison with available results has been presented. Extensions of the present study can be made into several directions. One extension concerns the generalization of the present results to non-hemispherical droplets [8,15]. In this case, one would apply the same procedure as discussed here but the equation set emerging from the imposition of the no-slip boundary on the plane wall needs to be solved numerically. Another interesting extension would be the possibility to study the transient deformation and asymptotic shapes of drop induced by an insoluble surfactant and also the effect of gravity. This is another case where it would be important to complement other numerical works present in the literature [12–15]. Finally, all results presented in this paper are also useful in the context of ensemble-averaging techniques to formulate effective boundary-condition problems [21–25], an issue which has been renewed recently because of its relevance in small-scale hydrodynamics [26, Chapt. 15].

Acknowledgements We are indebted to Prof. A. Prosperetti for proposing this problem and for his constant suggestions during the preparation of the manuscript. M. S. is grateful to B. M. Borkent for pertinent suggestions and STW (nanoned Programme) for financial support.

Appendix: Recurrence formulae

In this appendix we report the recurrence formulae to determine the coefficients A_{2n+1}, A_{2n}, G_{2n}, $\hat{A}_{2n-1}$, $\hat{A}_{2n}$, and $\hat{G}_{2n-2}$ for $n \geq 1$. The relevant boundary conditions at $r = 1$ are given by (13)–(18). Using the general representations (27)–(32), we can rewrite the boundary conditions and apply definite integrals for Legendre polynomials

$$\int_0^1 \mathrm{d}\mu \; P^m_{2n-1}(\mu) P^m_{2k-1}(\mu) = \frac{\delta_{nk}}{(4k-1)} \frac{(2k-1+m)!}{(2k-1-m)!},$$

$$\int_0^1 \mathrm{d}\mu \; P^m_{2n}(\mu) P^m_{2k}(\mu) = \frac{\delta_{nk}}{(4k+1)} \frac{(2k+m)!}{(2k-m)!},$$

$$\int_0^1 \mathrm{d}\mu \; P_{2n}(\mu) P_{2k-1}(\mu) = \frac{(-1)^{n+k}(2n-1)!!(2k-1)!!}{2(2n-2k+1)(n+k)(2n)!!(2k-2)!!},$$

$$\int_0^1 \mathrm{d}\mu \; P^1_{2n}(\mu) P^1_{2k-1}(\mu) = \frac{(-1)^{n+k}(2n+1)!!(2k-1)!!}{2(2n-2k+1)(n+k)(2n-2)!!(2k-2)!!},$$

$$\int_0^1 \mathrm{d}\mu \; P^2_{2n}(\mu) P^2_{2k-1}(\mu) = \frac{(-1)^{n+k}(2n+1)!!(2k+1)!!}{2(2n-2k+1)(n+k)(2n-2)!!(2k-4)!!}.$$

In this way, we can eliminate the summation for the even-order mode and finally obtain the recurrence formulae:

$$\frac{\delta_{k1}}{3} = \frac{(2k+1)}{2(4k-1)} A_{2k} + \frac{(k+1)(2k+3)(8k^2+6k-3)}{2k(2k+1)(4k+3)(4k+5)} A_{2k+2} + \frac{1}{2k(2k+1)} G_{2k+2} - \Delta_k \sum_{n=1}^{\infty} (n+1) \Lambda_{n,k} A_{2n+1},$$

$$
\begin{aligned}
\frac{\delta_{k1}}{3} &= \frac{(k-1)(2k-1)(4k^2+k-2)}{k(2k+1)(4k-3)(4k-1)}\hat{A}_{2k-2} + \frac{k}{4k+3}\hat{A}_{2k} + \frac{1}{2k(2k+1)}\hat{G}_{2k-2} - \Delta_k\sum_{n=1}^{\infty}(2n-1)\hat{\Lambda}_{n,k}\hat{A}_{2n-1},\\
&\quad \frac{6k^2-7k-2}{(2k-1)(4k-1)(4k+1)}A_{2k} + \frac{(2k+3)(6k^2+5k-3)}{2k(2k+1)(4k+3)(4k+5)}A_{2k+2} + \frac{1}{(2k-1)(4k-1)}G_{2k}\\
&\quad + \frac{(2k+3)}{2k(2k+1)(4k+3)}G_{2k+2} - \frac{\Delta_k}{(2k-1)(2k+2)}\sum_{n=1}^{\infty}(n-1)(2n+3)\Lambda_{n,k}A_{2n+1}\\
&= -\frac{(k-1)(6k^2+k-4)}{k(2k+1)(4k-3)(4k-1)}\hat{A}_{2k-2} - \frac{6k^2+13k+3}{2(k+1)(4k+1)(4k+3)}\hat{A}_{2k} + \frac{k-1}{k(2k+1)(4k-1)}\hat{G}_{2k-2}\\
&\quad + \frac{1}{2(k+1)(4k+3)}\hat{G}_{2k} + \frac{\Delta_k}{(k+1)(2k-1)}\sum_{n=1}^{\infty}(n-1)(2n+3)\hat{\Lambda}_{n,k}\hat{A}_{2n-1},\\
&\quad -\frac{2k^2(2k+1)}{(4k-1)(4k+1)}A_{2k} - \frac{(k+1)(2k+1)(2k+3)}{(4k+3)(4k+5)}A_{2k+2} + \frac{2k}{4k-1}G_{2k} + \frac{2k+1}{4k+3}G_{2k+2}\\
&\quad + \Delta_k\sum_{n=1}^{\infty}n(2n+1)\Lambda_{n,k}A_{2n+1}\\
&= \frac{2k(k-1)(2k-1)}{(4k-3)(4k-1)}\hat{A}_{2k-2} + \frac{k(2k+1)^2}{(4k+1)(4k+3)}\hat{A}_{2k} + \frac{2k}{4k-1}\hat{G}_{2k-2}\\
&\quad + \frac{2k+1}{4k+3}\hat{G}_{2k} - 2\Delta_k\sum_{n=1}^{\infty}n(2n+1)\hat{\Lambda}_{n,k}\hat{A}_{2n-1},\\
&\quad -\frac{(2k+1)(6k^2-7k-2)}{(2k-1)(4k-1)(4k+1)}A_{2k} - \frac{(2k+3)^2(6k^2+5k-3)}{2k(2k+1)(4k+3)(4k+5)}A_{2k+2} - \frac{(2k+1)}{(2k-1)(4k-1)}G_{2k}\\
&\quad - \frac{(2k+3)^2}{2k(2k+1)(4k+3)}G_{2k+2} + \frac{\Delta_k}{(k+1)(2k-1)}\sum_{n=1}^{\infty}(n-1)(n+1)(2n+3)\Lambda_{n,k}A_{2n+1}\\
&= \lambda\left\{-\frac{2(k-1)^2(6k^2+k-4)}{k(2k+1)(4k-3)(4k-1)}\hat{A}_{2k-2} - \frac{k(6k^2+13k+3)}{(k+1)(4k+1)(4k+3)}\hat{A}_{2k}\right.\\
&\qquad \left. + \frac{2(k-1)^2}{k(2k+1)(4k-1)}\hat{G}_{2k-2} + \frac{k}{(k+1)(4k+3)}\hat{G}_{2k}\right\}\\
&\quad + \frac{\lambda\Delta_k}{(k+1)(2k-1)}\sum_{n=1}^{\infty}(n-1)(2n-1)(2n+3)\hat{\Lambda}_{n,k}\hat{A}_{2n-1},\\
&\frac{2k^2(2k+1)^2}{(4k-1)(4k+1)}A_{2k} + \frac{(k+1)(2k+1)(2k+3)^2}{(4k+3)(4k+5)}A_{2k+2} - \frac{2k(2k+1)}{(4k-1)}G_{2k} - \frac{(2k+1)(2k+3)}{(4k+3)}G_{2k+2}\\
&\quad -2\Delta_k\sum_{n=1}^{\infty}n(n+1)(2n+1)\Lambda_{n,k}A_{2n+1}\\
&= \lambda\left\{\frac{4k(k-1)^2(2k-1)}{(4k-3)(4k-1)}\hat{A}_{2k-2} + \frac{2k^2(2k+1)^2}{(4k+1)(4k+3)}\hat{A}_{2k} + \frac{4k(k-1)}{4k-1}\hat{G}_{2k-2} + \frac{2k(2k+1)}{4k+3}\hat{G}_{2k}\right\}\\
&\quad -2\lambda\Delta_k\sum_{n=1}^{\infty}n(2n-1)(2n+1)\hat{\Lambda}_{n,k}\hat{A}_{2n-1},
\end{aligned}
$$

where we have used

$$
\Lambda_{n,k} = \frac{(-1)^n(2n+1)!!}{2(2n-2k-1)(2n-2k+1)(n+k)(n+k+1)(2n)!!},
$$

$$\hat{\Lambda}_{n,k} = \frac{(-1)^n (2n-1)!!}{4(2n-2k-1)(2n-2k+1)(n+k)(n+k+1)(2n-2)!!},$$

and

$$\Delta_k = \frac{(-1)^k (4k+1)(2k-1)!!}{(2k)!!}.$$

References

1. De Gennes PG, Brochard-Wyart F, Quere D (2003) Capillarity and wetting phenomena: drops, bubbles, pearls, waves. Springer
2. MacCann DJ, Prince RGH (1971) Regimes of bubbling at a submerged orifice. Chem Eng Sci 26:1505–1512
3. Duhar G, Collin C (2004) A predictive model for the detachment of bubbles injected in a viscous shear flow with small inertial effects. Phys Fluids 16:L31–L34
4. Chatterjee J (2001) A criterion for buoyancy induced drop detachment based on an analytical approximation of the drop shape. Colloid Surf A Physiochem Eng Asp 178:249–263
5. O'Neill ME (1968) A Sphere in contact with a plane wall in a slow linear shear flow. Chem Eng Sci 23:1293–1298
6. Hyman WA (1972) Shear flow over a protrusion from a plane wall. J Biomech 5:45–48. Corrigendam on p 643
7. Price TC (1985) Slow linear flow past a hemispherical bump in a plane wall. Q J Mech Appl Math 38:93–104
8. Pozrikidis C (1997) Shear flow over a protuberance on a plane wall. J Eng Math 31:29–42
9. Dussan VEB, Chow RT-P (1983) On the ability of drops or bubbles to stick to non-horizontal surfaces of solids. J Fluid Mech 137:1–29
10. Dussan VEB (1985) On the ability of drops or bubbles to stick to non-horizontal surfaces of solids. Part 2. Small drops or bubbles having contact angles of arbitrary size. J Fluid Mech 151:1–20
11. Dussan VEB (1987) On the ability of drops or bubbles to stick to surface of solids. Part 3. The influence of the motion of the surrounding fluid on dislodging drops. J Fluid Mech 174:381–397
12. Dimitrakopoulos P, Higdon JJL (1997) Displacement of fluid droplets from solid surfaces in low-Reynolds number shear flows. J Fluid Mech 336:351–378
13. Dimitrakopoulos P, Higdon JJL (1998) On the displacement of three dimensional fluid droplets from solid surfaces in low-Reynolds number shear flows. J Fluid Mech 377:189–222
14. Li X, Pozrikidis C (1996) Shear flow over a liquid drop adhering to a solid surface. J Fluid Mech 307:167–190
15. Yon S, Pozrikidis C (1999) Deformation of a liquid drop adhering to a plane wall: significance of the drop viscosity and the effect of an insoluble surfactant. Phys Fluids 11:1297–1308
16. Schleizer AD, Bonnecaze RT (1999) Displacement of a two-dimensional immiscibile droplet adhering to a wall in shear and pressure-driven flows. J Fluid Mech 383:29–54
17. Spelt PDM (2006) Shear flow past two-dimensional droplets pinned or moving on an adhering channel wall at moderate Reynolds numbers: a numerical study. J Fluid Mech 561:439–463
18. Chan C-H, Leal LG (1979) The motion of a deformable drop in a second-order fluid. J Fluid Mech 92:131–170
19. Magnaudet J, Takagi S, Legendre D (2003) Drag, deformation and lateral migration of a buoyant drop moving near a wall. J Fluid Mech 476:115–157
20. Taylor GI (1931) The viscosity of a fluid containing small drops of another fluid. Proc R Soc Lond A 138:41–48
21. Sarkar K, Prosperetti A (1996) Effective boundary conditions for Stokes flow over a rough surface. J Fluid Mech 316:223–240
22. Sbragaglia M, Prosperetti A (2007) Effective velocity boundary condition at a mixed slip surface. J Fluid Mech 578:435–451
23. Lauga E, Stone HA (2003) Effective slip in pressure-driven Stokes flow. J Fluid Mech 489:55–77
24. Benzi R, Biferale L, Sbragaglia M, Succi S, Toschi F (2006) Mesoscopic modelling of heterogeneous boundary conditions for microchannel flows. J Fluid Mech 548:257–280
25. Sbragaglia M, Sugiyama K (2007) Boundary induced non-linearities at small Reynolds numbers. Physica D 228:140–147
26. Lauga E, Brenner M, Stone H (2007) Microfluidics: the no-slip boundary condition. Handbook of experimental fluid dynamics, Springer.